

## THERMAL ANALYSIS OF AN ELECTRIC AIRCRAFT TAIL ROTOR

IOAN-DRAGOȘ DEACONU, VALENTIN NĂVRĂPESCU, AUREL-IONUȚ CHIRILĂ

**Key words:** Thermal analysis, Heat transfer Coefficient, Aircraft, Tail rotor, Electric motor, Green transportation, Computational fluid dynamics (CFD).

The replacement of petrol engines that have CO<sub>2</sub> emissions with electric motors is a viable solution for green transportation. The study shows thermal analysis of the tail rotor hub of an electric tail rotor aircraft in order to correctly design the driving system with respect to heat stress during the operation of the aircraft. The study results refer to the heat transfer coefficient of the tail rotor hub acting as a heat sink for the electric tail rotor motor. Thermal analysis is performed using finite volume method and incorporates the applied mathematical model, considerations and boundary value conditions.

### 1. INTRODUCTION

The global warming issue is a major threat [1–3]. Significant contributions to this effect are the CO<sub>2</sub> emissions that primarily come from combustion of petroleum-based products, *e.g.* gasoline, which is the energy source for internal combustion engines [4, 5]. As the CO<sub>2</sub> emissions continue to increase [6–7] designing an aircraft that pollutes less is valuable.

An efficient solution is to embrace a new approach to the existing tail rotor driving chain by replacing it with a direct driving electric motor. In [8] it is described such a direct driving motor of transverse flux type with permanent magnets.

Whatever the type of electric motor, thermal phenomena is crucial. The reason is temperature dependent materials properties, *e.g.* insulation materials, which are used for the manufacturing the windings of the electric motor.

It is proven by experiments that any temperature rise above the maximum limit of the material conducts to physical irreversible changes, thus consuming the lifetime of the machine [9].

Studies regarding the thermal analysis of a helicopter are found in [10, 11] where the helicopter infrared (IR) radiation intensity is computed, while considering the hovering state and various airframe emissivities.

The electric motor that drives the tail rotor is characterized by a power density of about one unit of kilowatt per motor kilogram, given the efficiency larger than ninety percent. In consequence, the cooling of the electric tail rotor motor must be efficient.

The housing of the motor is in contact with the tail rotor hub (*i.e.* electric motor mounting place), which behaves like a heat sink.

The aim of the study is to compute the heat transfer coefficient of the tail rotor hub found on the boom tail.

### 2. GEOMETRY MODEL

In Fig. 1 is presented the studied aircraft boom tail. One thermal analysis approach of the electric tail rotor motor is based on lumped-parameter thermal networks [12]. This method allows the modelling of all heat transfer modes: conduction, convection and radiation.

For the computation of the network parameters accounting for heat transfer by conduction and radiation mode, it is possible to apply mathematical reasoning.

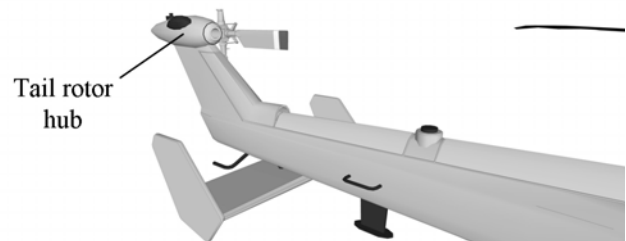


Fig. 1 – Initial geometry of the aircraft boom tail.

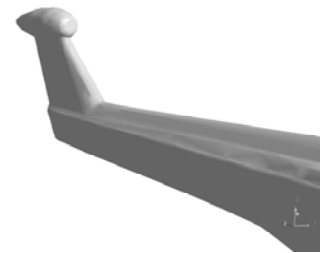


Fig. 2 – Final simplified geometry of the aircraft boom tail.

In case of the convective heat transfer mode, empiric mathematical laws are considered which are based on dimensional analysis and similitude criterion [13].

Such approach is suitable for simple geometries, such as: plates, cylinders, spheres *etc.* The given geometry of the tail rotor hub and boom tail is complex and difficult to be divided into simple geometries.

For better results regarding the heat transfer coefficient of the tail rotor hub, a more appropriate approach is to apply computational fluid dynamics combined with conjugated heat transfer numeric algorithms using finite volumes method implemented within the ANSYS CFX, CFD code [14].

The initial geometry of the boom tail model involves significant computational resources, *i.e.* time and computer hardware. For better performances a simplified model is used [15], which is presented in Fig. 2.

In [16] is shown that the main rotor induces a distinctive turbulence of the rotor wake in the region between hub and tail boom.

The control rods have cylindrical shape and the formation of a von Kármán vortex street is present. The induced turbulence improves the cooling of the tail rotor hub. Such positive effects in terms of increased heat removal are neglected in this study by not considering the main rotor and considering a steady-state flowing regime.

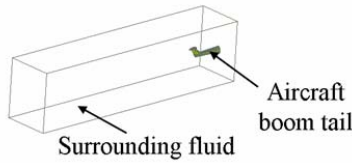


Fig. 3 – The overall view of the implemented geometry model

In Fig. 3 is depicted an overall view of the considered model.

### 3. MATHEMATICAL MODEL

In case of aircrafts the flow of the fluid can be compressible, *i.e.* the fluid density has an important gradient due to significant pressure gradient.

There is a dimensionless criterion that allows for the compressibility of the fluid flow assessment. This criterion is defined by the Mach number, as follows [17]:

$$Ma = u \cdot a^{-1}, \quad (1)$$

where  $u$  [m/s] is the fluid speed and  $a$  [m/s] is the speed of sound. For the given study conditions it follows that the flow is subsonic.

The equations describing the steady-state solution of the coupled problems, fluid flow and conjugated heat transfer, are the following [18].

For fluid flow problem, the transport equation of mass or the continuity equation is defined as:

$$\nabla \cdot (\rho \mathbf{u}) = 0, \quad (2)$$

where  $\rho$  [kg/m<sup>3</sup>] is fluid's mass density and  $\mathbf{u}$  [m/s] is velocity.

The transport equation of the momentum (Navier-Stokes equation) is:

$$\rho[(\mathbf{u} \cdot \nabla)\mathbf{u}] = -\nabla p + \mu \Delta \mathbf{u}, \quad (3)$$

where  $p$  [Pa] is pressure,  $\mu$  [kg/m/s] is dynamic viscosity of the fluid,  $\Delta$  is Laplace operator.

The conjugated heat transfer problem coupled with the fluid mechanics is modelled by thermal energy equation.

For the tail rotor hub the equation is

$$\dot{q} = \nabla \cdot (-k \nabla T), \quad (4)$$

for the rest of the boom tail (without the tail rotor hub) the equation is:

$$0 = \nabla \cdot (-k \nabla T), \quad (5)$$

while for the fluid domain is:

$$\rho C_p \mathbf{u} \cdot \nabla T = \nabla \cdot (k \nabla T) \quad (6)$$

where  $C_p$  [J/kg/K] is specific heat at constant pressure,  $k$  [W/m/K] is thermal conductivity,  $\dot{q}$  [W/m<sup>3</sup>] rate of energy generation and  $T$  [K] is temperature.

The fluid density is computed using the ANSYS's CFX built in ideal gas equation [19]:

$$\rho = \frac{M \cdot p}{R \cdot T}, \quad (8)$$

where  $M$  [g/mol] is molar mass,  $R$  [J/mol/K] is the universal gas constant and the rest of the quantities are similar to previous equations.

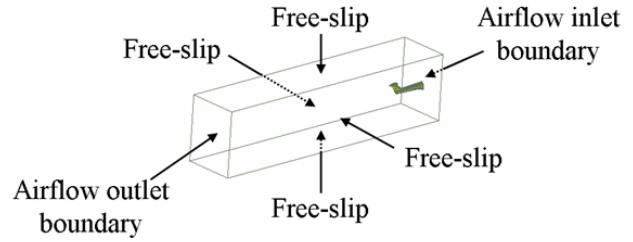


Fig. 4 – Computational domain.

### 4. NUMERICAL MODEL

The study is performed for various flow velocities between 10 m/s to 80 m/s.

The boundary values definitions for the fluid mechanics problem are shown in Fig. 4. At the inlet it is considered a normal inflow velocity, while at the outlet an open boundary condition is set.

The remaining sides of the enclosure are free-slip type. Regarding the heat transfer problem, as boundary conditions it is set a temperature of 40°C for the environment. The natural convection heat transfer mode is not considered due to the much more intensive forced convection heat transfer mode.

The heat source of the model is given by the active power losses generated by the electric tail rotor motor, which is located inside the tail rotor hub. The total amount of total losses is evaluated by experiment using the efficiency characteristics [20, 21].

The finite volumes method requires that the computational domains are meshed into small volumes. In Fig. 5 is presented the resulting mesh projected on the symmetry plane of the model. As the tail rotor hub's convective heat transfer is the main objective of the study then a finer mesh around this surface is required. Inflation layers are present in order to correctly solve for the thermal boundary layer and the velocity boundary layer respectively. The model has a total number of 2 230 099 linear elements.

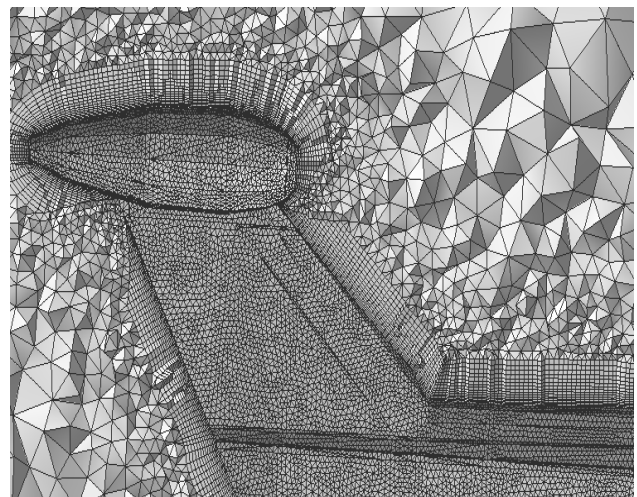


Fig. 5 – Mesh zoomed on aircraft tail rotor hub (symmetry plane).

### 5. RESULTS

The final results are obtained by numeric integration of the boundary value problem described by (2)–(4).

While the model is three-dimensional the results are depicted on the middle plane section of model.

The relative pressure field for a velocity of 80 m/s is presented in Fig. 6 and Fig. 7, side view and from above respectively. It can be observed that the leading (inflow) edges of the tail rotor hub are stressed more due to the increased pressure.

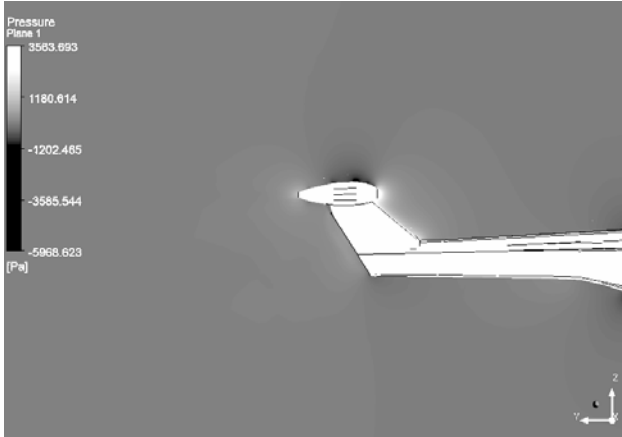


Fig. 6 – Relative pressure field for 80 m/s (side view).

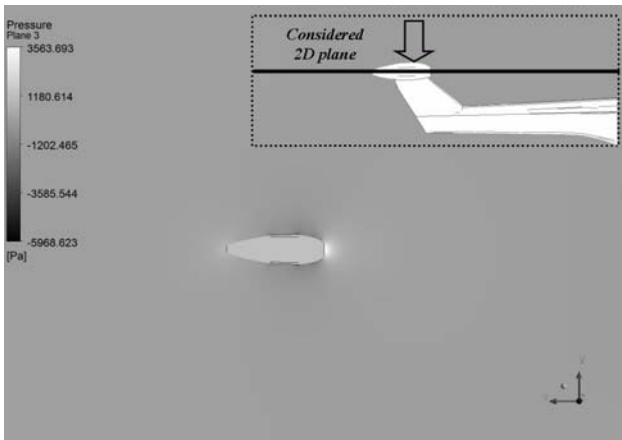


Fig. 7 – Relative pressure field for 80 m/s (top view).

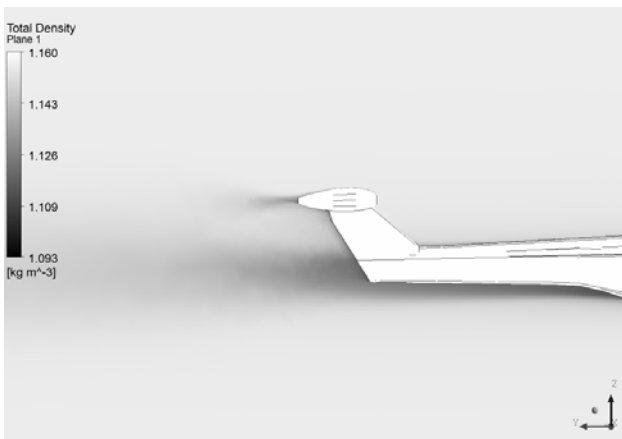


Fig. 8 – Air density field for 80 m/s (side view).

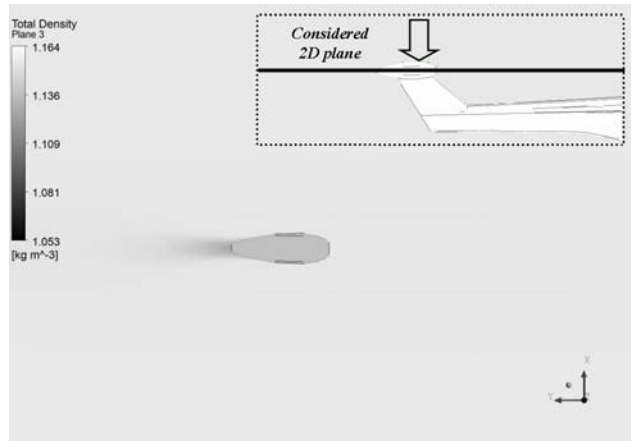


Fig. 9 – Air density field for 80 m/s (top view).

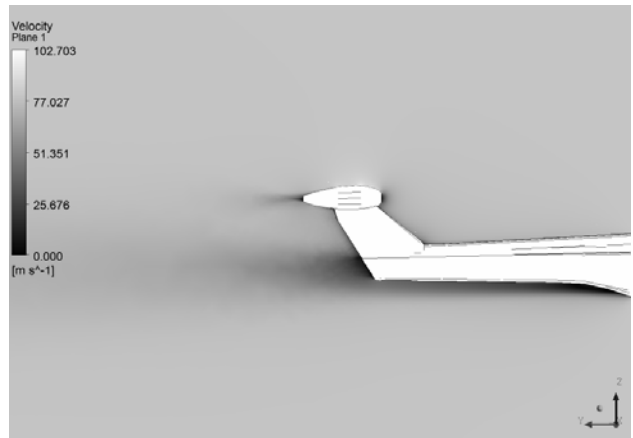


Fig. 10 – Velocity magnitude field for an inflow of 80 m/s (side view).

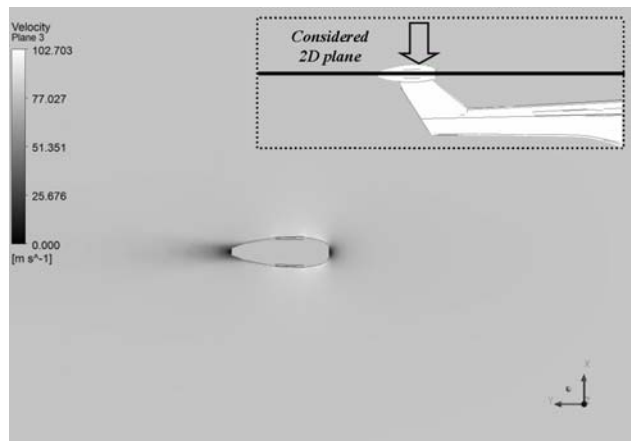


Fig. 11 – Velocity magnitude field for an inflow of 80 m/s (top view).

As the pressure is referred to atmospheric pressure, the positive values signify an increased pressure, while the negative values signify a decreased pressure, as it is the case of the trailing (outflow) edges of the model. The maximum pressure is about 3.5 % above the atmospheric one, while the minimum pressure is about 5.6 % below the atmospheric pressure.

In Fig. 8 and Fig. 9 is depicted the field of the air density flowing around the aircraft during the flight, for the same velocity of 80 m/s, side view and top view respectively. As expected, due to small pressure gradient, the fluid density also registers a small gradient.

The two results indicate an incompressible flow, but a genuine indicator of this regime is the Mach number.

Based on the resulted velocity field, depicted in Fig. 10 and Fig. 11 (side and top view respectively), within the whole computational domain, the Ma number is below 0.3. Thus, it is confirmed that the flow is indeed incompressible.

The heat transfer does not occur in the same amount over the entire surface. Instead, the heat transfer is a local phenomenon specific to each particular infinitesimal surface element.

For a global characterization of the tail rotor hub's surface convective heat transfer mode an average heat transfer coefficient is computed, which is defined by:

$$\bar{h} = \frac{1}{S} \iint_S h_S \cdot dS \quad (9)$$

where  $h_S$  [W/m<sup>2</sup>/K] is local heat transfer coefficient and  $S$  [m<sup>2</sup>] is the tail rotor hub's surface, which is in contact with the surrounding flowing fluid.

The local heat transfer coefficient is defined as:

$$h_S = \frac{\dot{q}_S}{dS \cdot (T_s - T_0)}, \quad (10)$$

where  $\dot{q}_S$  [W] is local heat source,  $dS$  [m<sup>2</sup>] is local infinitesimal surface,  $T_s$  [K] is local temperature of the infinitesimal surface and  $T_0$  [K] is the far-field temperature.

In Fig. 12 is presented the relationship with the fluid velocity. It is observed that the overall trend is an increased value of the heat transfer coefficient as the faster the aircraft is moving.

Up to about 40 m/s the relationship is linear. Above this value the formation of a plateau is starting to develop.

## 6. CONCLUSIONS

As the trend is to replace the tail rotor engine with an electric motor, the cooling improvement of such motor is a requirement in order to obtain high-performance electric driving motors with less weight.

One solution is to take advantage of the existing tail rotor hub where the electric motor resides and using it as a heat-sink. In this vein a thermal analysis on the convective heat transfer coefficient of an aircraft's tail rotor hub is presented.

The results are useful for further thermal analysis using thermal circuit network approach. Based on the surface's average heat transfer coefficient a non-linear thermal resistance characterising the convective heat transfer is obtainable.

It must be underlined that the obtained heat transfer coefficient values are a worst-case situation by considering a steady-state flow. During real operation there are additional factors that positively influence the heat removal process and have not been considered. One of these is the main rotor that induces unsteady flow registered as von Kármán vortex street, due to its rotor blade tips and cylindrical cross-section control rods. This flow behind the main rotor strongly influences the cooling behaviour of downstream placed parts, such as the tail rotor hub. Another one is the tail rotor wake. Its blade tips also induce flow instabilities that improve the heat transfer phenomenon. Regarding the direct cooling of the electric motor, the tail rotor hub is provided with cooling vents in order to improve the evacuation of the

warm air and the intake of the cold one. A last one is thermal radiation heat transfer mode that has been neglected.

Received on March 4, 2018

## REFERENCES

1. National Geographic, *The planet is heating up—and fast*, What Is Global Warming? ([www.nationalgeographic.com/environment/global-warming/global-warming-overview/](http://www.nationalgeographic.com/environment/global-warming/global-warming-overview/)), Accessed January 12, 2018.
2. Intergovernmental Panel on Climate Change, *What is the IPCC?*, IPCC Factsheet ([climate.nasa.gov/evidence/](http://climate.nasa.gov/evidence/)), August 30, 2013.
3. Union of Concerned Scientists, *Why does CO2 get most of the attention when there are so many other heat-trapping gases?*, Science for a healthy planet and safer world ([www.ucsusa.org/global-warming/science-and-impacts/science/CO2-and-global-warming-faq.html](http://www.ucsusa.org/global-warming/science-and-impacts/science/CO2-and-global-warming-faq.html)), Accessed January 14, 2018.
4. Environmental Protection Agency, *Sources of Greenhouse Gas Emissions – Transportation Sector Emissions*, Greenhouse Gas Emissions ([www.epa.gov/ghgemissions/sources-greenhouse-gas-emissions](http://www.epa.gov/ghgemissions/sources-greenhouse-gas-emissions)), Accessed on January 02, 2018.
5. European Environment Agency, *Share of transport GHG emissions*, Greenhouse gas emissions from transport ([www.eea.europa.eu/data-and-maps/indicators/transport-emissions-of-greenhouse-gases/transport-emissions-of-greenhouse-gases-10](http://www.eea.europa.eu/data-and-maps/indicators/transport-emissions-of-greenhouse-gases/transport-emissions-of-greenhouse-gases-10)), Accessed on January 02, 2018.
6. Intergovernmental Panel on Climate Change, *Climate Change 2014, Synthesis Report*, ([www.ipcc.ch/pdf/assessment-report/ar5/syr](http://www.ipcc.ch/pdf/assessment-report/ar5/syr)) Accessed January 14, 2018.
7. NASA, *Climate change: How do we know?*, Global Climate Change - Vital Signs of the Planet – Facts (<https://climate.nasa.gov/evidence>), Accessed January 16, 2018.
8. Y. Zhou, Y. Han, Y. Mi, L. Chen, *The design of transverse flux PMDCM for electric direct driving (Aeronautic transmissions)*, CRC Press/Balkema (Edit.), Power Transmissions, pp. 39-44, Taylor & Francis Group, London, 2017.
9. R. Rothe, L. Hameyer, *Life Expectancy Calculation for Electric Vehicle Traction Motors Regarding Dynamic Temperature and Driving Cycles*, The IEEE International Electric Machines and Drives Conference (IEMDC 2011), Niagara Falls, Canada, 2011.
10. C. Pan, J. Zhang, Y. Shan, *Modeling and Analysis of Helicopter Thermal and Infrared Radiation*, Chinese Journal of Aeronautics, **24**, 5, pp. 558–567 (2011).
11. Y. Li, Y. Xuan, *Thermal characteristics of helicopters based on integrated fuselage structure/engine model*, International Journal of Heat and Mass Transfer, **115**, A, pp. 102–114 (2017).
12. Y. A. Cengel, *Heat Transfer: A Practical Approach*, (2<sup>nd</sup> Ed.), McGraw-Hill, 2003, pp. 131–155.
13. B. Zohuri, *Dimensional Analysis and Self-Similarity Methods for Engineers and Scientists*, Springer International Publishing, Switzerland, 2015, pp. 93–193.
14. ANSYS, Inc. – *ANSYS CFX Release 15.0*, ([www.ansys.com/products/fluids/ansys-cfx](http://www.ansys.com/products/fluids/ansys-cfx)), 2013.
15. P. Beaumier, J. M. Bousquet, *Applied CFD for analysing aerodynamic flows around helicopters*, 24th International Congress of the Aeronautical Sciences (ICAS 2004), Yokohama, Japan, pp. 1–10.
16. U. Kowarsch, M. Keßler, E. Kramer, *CFD-Simulation of the rotor head influence to the rotor-fuselage interaction*, European Rotorcraft Forum, pp. 1–12 (2014).
17. J. Ackeret, *Der Luftwiderstand bei sehr grossen Geschwindigkeiten*, Schweizerische Bauzeitung, **94**, 15, 12 Oktober 1929.
18. F. P. Incropera, D. P. DeWitt, T. L. Bergman, A. S. Lavine, *Fundamentals of Heat and Mass Transfer* (6<sup>th</sup> ed.), John Wiley & Sons, 2007.
19. ANSYS® Academic Research CFD, Release 15.0, Help System, *CFX Solver – Theory Guide*, ANSYS, Inc., 2013.
20. E. Cazacu, V. Năvrănescu, I.V. Nemoianu, *On-site efficiency evaluation for in-service induction motors. Part I: Électrotechnique et électroénergétique*, Rev. Roum. Sci. Techn. – Électrotechn. et Énerg., **58**, 1, pp. 63–72 (2013).
21. Veronica Mănescu (Păltănea), G. Păltănea, H. Gavrilă, G. Scutaru, I. Peter, *High efficiency electrical motors state of the art and challenges. Part I: Électrotechnique et électroénergétique*, Rev. Roum. Sci. Techn. – Électrotechn. et Énerg., **62**, 1, pp. 14–18 (2017).